THE JOURNAL OF PHYSICAL CHEMISTRY B

 VOLUME 106, NUMBER 43, OCTOBER 31, 2002

LETTERS

In Situ AFM Studies of Metal Deposition

Michael E. Hyde, Robert Jacobs, and Richard G. Compton*

Physical and Theoretical Chemistry Laboratory, University of Oxford, South Parks Road, Oxford, OX1 3QZ, United Kingdom

Received: June 6, 2002; In Final Form: July 30, 2002

In-situ AFM has been used to *directly* study the growth of individual lead nuclei on a highly boron doped diamond electrode and the rates at which they appear as a function of time and overpotential. This method represents a new approach to the study of these processes, previously only possible indirectly via comparison of potentiostatic current transients with models such as that of Scharifker and Mostany (Journal of Electroanalytical Chemistry, **1984**, *177*, 13). It therefore allows the assumptions made by these models to be tested in an independent manner. At high overpotentials, it is found that the growth rate of the nuclei is close to that predicted assuming diffusion control, a result representing the first direct verification that this is in fact the case using a method independent of current transient analysis. A re-expression for the Scharifker and Mostany equation for the current density, an improvement in that it allows less equivocal interpretation of the results, is suggested, and the nucleation rate derived from it compared with that determined directly by AFM. A very good agreement is found, demonstrating the validity of the in-situ AFM approach in this case, and also suggesting that the assumptions made by the Scharifker and Mostany model are substantially correct.

Introduction

The experiments described in this paper were designed to use in-situ AFM to directly image the electrodeposition process at a micron scale and so allow calculation of nucleation and nucleus growth rates as a function of time and/or overpotential. This approach allows a direct comparison between the parameters extracted from analysis of current transients and the actual processes observed to be occurring on the electrode surface.

The use of in-situ AFM to study the electrodeposition of metals has very considerable advantages over traditional ex-situ methods.[1] In-situ techniques allow the structure of the surface to be probed directly, without the need for removal of the electrode from solution, thereby avoiding any morphological changes that may occur on drying. Also, changes in the properties of a single area as a function of time may be studied, which is impossible when using ex-situ techniques.

In-situ SPM is a well-established technique,[2] but until now, studies of electrodeposition have almost exclusively focused on the use of crystallographic metal planes as electrodes, and the atomic scale appearance of electrochemically deposited adatoms.[3−8]

Current transient analysis is the standard way of determining nucleation rates and saturation nucleus densities. It is an indirect method in the sense that it relies on comparison of the experimental transients with theoretical expressions for the current density, such as that derived by Scharifker and Mostany.[9] There are presently several competing models,[10−12] based on differing assumptions.

The experiments described below therefore represent a new approach to the analysis of metal deposition, such as for example may be relevant to electroplating or electrowinning of metals, as they allow the validity of the assumptions made by these theoretical models to be independently tested.

* To whom correspondence should be addressed. Tel: 01865 275413. Fax: 01865 275410. E-mail: richard.compton@chemistry.ox.ac.uk.

10.1021/jp0213607 CCC: $22.00
Published on Web 10/03/2002

Experimental Section

All reagents were of analytical grade, and used without further purification. The reagents used were: lead (II) nitrate (Aldrich, 99%+), and potassium nitrate (BDH AnalaR, 99.5%+). Solutions were prepared using water with a resistivity of not less than 18 MΩcm, using an Elgastat (Elga, Bucks, U.K.) UHQ grade water purification system. In all cases, experiments were performed in a solution containing 500 μM $Pb(NO_3)_2$ and 1M KNO_3.

The working electrode chosen was boron doped diamond. The prepolished BDD film (5 × 5 × 0.535 mm, resistance approximately 0.4 Ω), grown on graphite by chemical vapor deposition, was supplied by DeBeers Industrial Diamond Division (Ascot, U.K.). It was pressed into a PTFE mounting, and an electrical connection made to a metal stub on the rear of the mounting using silver-loaded epoxy resin (RS). Before each set of measurements, the electrode was polished with 1 μm diamond polishing compound (Kemet, U.K.) to dislodge any surface residue, then sonicated in UHQ water for 30 min to remove as much material from the surface as possible.

This system was chosen after careful consideration and preliminary investigation of various metals and electrodes including cobalt and zinc at different concentrations on glassy carbon and BDD; lead on BDD was found to have a relatively low nucleation rate, facilitating its measurement by both chronoamperometry and AFM. Experiments (not reported in this paper) on glassy carbon showed that its irregular surface and poor reproducibility made it unsuitable for use as a substrate, whereas BDD was chosen for its extremely flat surface (having a height variation of only ~5 nm over 5 × 5 μm areas). This uniformity was extremely useful in the distinguishing of nuclei from the electrode surface.

One potential disadvantage of BDD, however, was that it was found to have areas of relatively low and high conductivity, visible as light and dark areas respectively under an optical microscope, which potentially made generalizations from the area studied to the whole electrode difficult. This problem was avoided by scanning an area large enough to span both types of surface.

Experiments were performed in a Digital Instruments TappingMode fluid cell (having an approximate volume 0.5 mL), using a standard three electrode configuration. Once in position on the AFM scanner head, the solution was fed into one of the inlets of the cell using a syringe until it was full and no bubbles remained. One of the other inlets had the platinum counter electrode placed in it, and the third was used as a fluid outlet. The outlet tube was clipped shut, and the partly filled input syringe used as a reservoir, into which the calomel reference electrode (Radiometer, Copenhagen, Denmark) was placed. This configuration meant that there was a relatively large solution distance between the working and reference electrodes. However, the low resistivity of the solution usually made the resulting ohmic drop acceptable (see later).

The microscope used was a Digital Instruments (Santa Barbara, CA) Multimode SPM, operating in TappingMode with a "J" scanner, having a lateral range of 125 × 125 μm and a vertical range of 5 μm. Standard silicon nitride probes (model NP), having a force constant of approximately 0.58 Nm^{-1} were used. Contact mode, despite its better lateral resolution, was found to be unsuitable, as it physically removed any deposits from the area being scanned. This was demonstrated using optical microscopy: after scanning while simultaneously depositing for an extended period, withdrawal of the tip leaves a clearly visible clean area. This effect has also been reported in the literature.[13] No such removal was observed in TappingMode, and in fact smearing of images due to dragging of material across the surface was minimized.

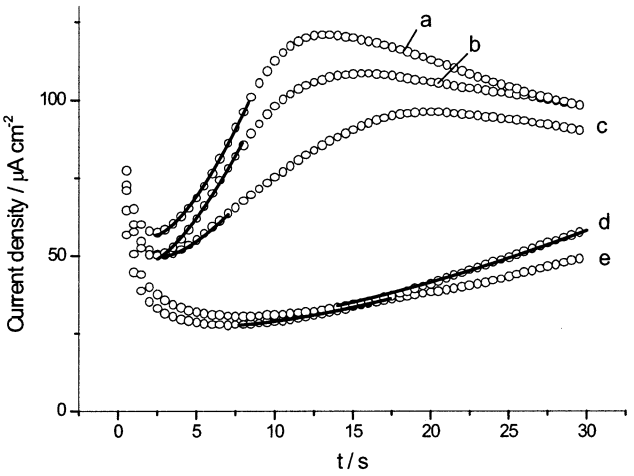

Figure 1. Experimental (open circles) and optimized fits (lines) of the potentiostatic transient for the lead system, performed at (a) −0.73 V, (b) −0.70 V, (c) −0.67 V, (d) −0.63 V, (e) −0.60 V.

Results and Discussion

Voltammetric Analysis. The deposition from a 500 μM Pb^{2+} solution on to boron doped diamond was initially studied using cyclic voltammetry. It was determined that at a scan rate of 50 mVs^{-1} deposition started to occur at approximately −0.62 V. A sharp stripping peak was observed at −0.47 V, and the formal potential of the Pb/Pb^{2+} couple was found to be −0.52 V, as revealed by the "crossover point" on the cyclic voltammogram.[14]

An analysis of the chronoamperometric transients was therefore initially performed at potentials of between −0.63 V and −0.76 V vs SCE, to identify the potentials at which to deposit. The resulting data are shown in Figure 1. As expected, they show rising transients followed by decay toward a constant current, with the peaks appearing earlier and having higher maxima at elevated overpotentials.

Analysis of these data was initially performed using the Scharifker and Mostany result for the current density[9]

$$I(t) = zFc\left(\frac{D}{\pi t}\right)^{1/2}\{1 - \exp[-\alpha(At - 1 + e^{-At})]\} \qquad (1)$$

in which

$$\alpha = (2\pi)^{3/2}D\left(\frac{cM}{\rho}\right)^{1/2}\frac{N_0}{A}$$

c is the solution concentration, D is the diffusion coefficient of the depositing species, t is the time after the potential step was applied, A is the nucleation rate expressed as an appearance rate per active site per second, M is the molar mass of the depositing species, ρ is the density of the depositing species, and N_0 is the saturation nucleus density (the number of active sites).

At present, there is considerable debate about the validity and accuracy of the Scharifker and Mostany model compared to for example the models of Sluyters-Rehbach, Wijenberg, Bosco and Sluyters,[10] and Mirkin and Nilov.[11,15−17] In practice, however, it was found that computational curve fitting of eq 1 to the experimental data using Microcal Origin software produced good fits. On the other hand, no convergence to a

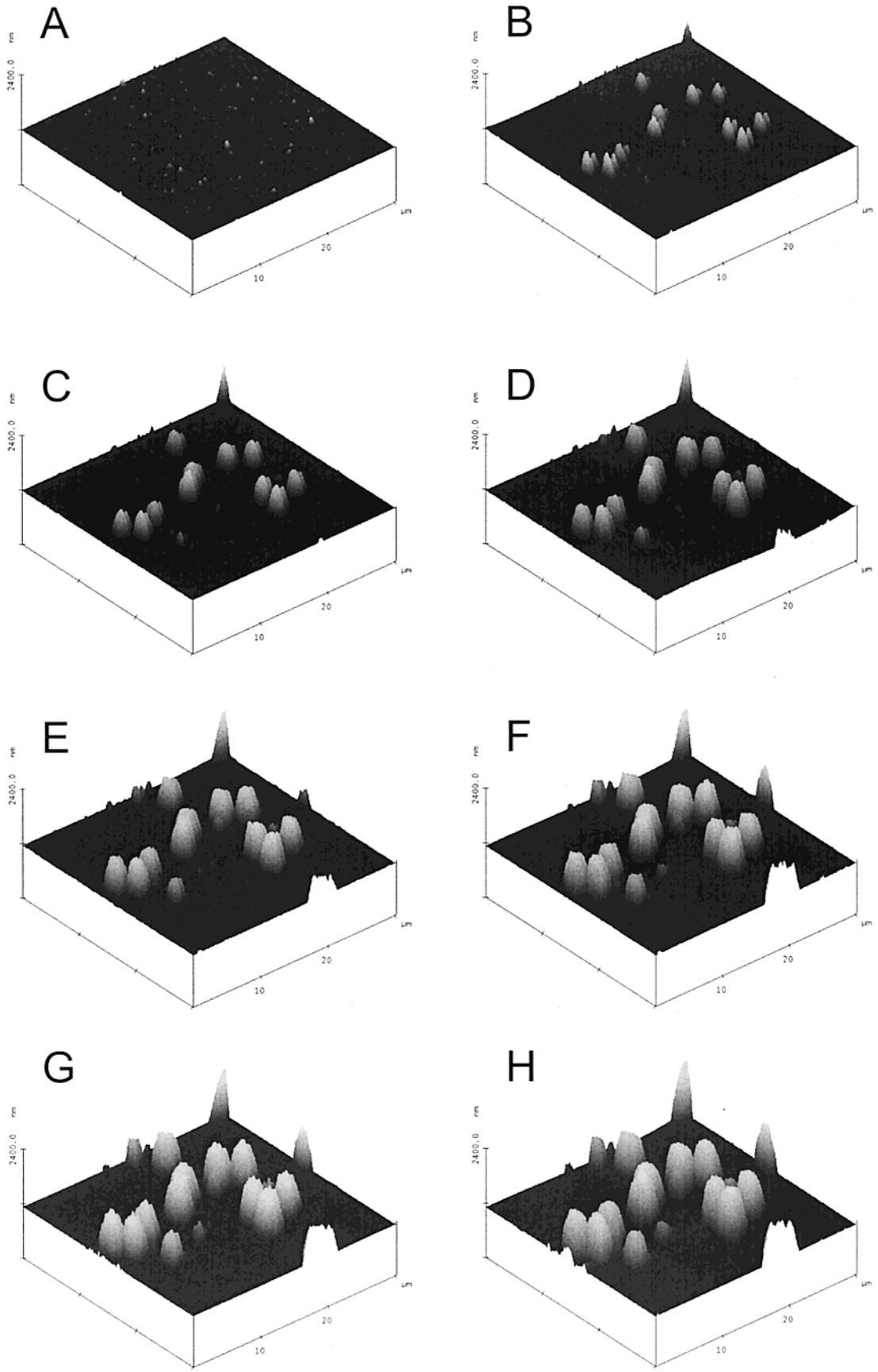

Figure 2. Successive in-situ images of lead nuclei growing on a BDD electrode at a potential of −0.70 V. Deposition times: (A) clean electrode, (B) 20 s, (C) 40 s, (D) 60 s, (E) 80 s, (F) 120 s, (G) 140 s, and (H) 160 s.

specific set of parameters could be obtained; a range of good fits having various values of α and A were found.

The following procedure was therefore used to resolve this uncertainty.

TABLE 1: Optimized Values of t_0 and I_0 Derived from Analysis of Potentiostatic Transients

potential/V	t_0/s	I_0/μAcm^{-2}
−0.63	16.5	20
−0.67	6.8	30
−0.70	3.0	50
−0.73	1.7	50
−0.76	2.4	60

Consider the SM result for the current (eq 1). In principle, this describes the entire current response. However, the only part of the response of interest in terms of nucleation rate and saturation nuclear density is the initial rising transient, which occurs at small values of At. We can therefore make use of the approximation $(1 - e^{-x}) = x$, which gives

$$I = zFc\left(\frac{D}{\pi t}\right)^{1/2}[\alpha(At - 1 + e^{-At})] \quad (2)$$

If e^{-At} is then expressed as a series expansion, we have

$$I = zFc\left(\frac{D}{\pi t}\right)^{1/2}\left[\alpha\left(\frac{A^2t^2}{2} + ...\right)\right] \quad (3)$$

Inserting the full value of α then gives

$$I = \left[2^{1/2}zFc\pi D^{3/2}\left(\frac{Mc}{\rho}\right)^{1/2}N_0A\right].t^{3/2} \quad (4)$$

Thus, the rising transient must fit a $t^{3/2}$ curve, with a proportionality constant containing N_0 and A. In fact, this takes no account of induction time, t_0, between the double layer charging and nucleation beginning,[18] or the baseline current, I_0. The full expression used to fit to the rising transients was therefore

$$I = I_0 + k(t - t_0)^{3/2} \quad (5)$$

where k is the square bracketed term in eq 4.

This expression was found to fit well in all cases (Figure 1), with physically reasonable values of t_0 and I_0, the values of which are shown in Table 1. The values of k derived from this analysis were then divided by the constant terms in eq 4, using a value of 1.0×10^{-5} cm^{2}s^{-1} for D,[19] to give values of N_0A. These values are compared with those derived from AFM experiments in Table 2.

In-situ AFM

In-situ measurements were taken at potentials of −0.63 V, −0.67 V, −0.70 V, and −0.73 V, a range designed to extend from complete charge control to complete diffusion control. In all cases, the scanner was engaged and allowed to scan a 30 × 30 μm area at a scan rate of 1 Hz (using a resolution of 256 lines per scan). The slow scan axis was then disabled, so the AFM tip moved across only one line at the edge of the image. A potential pulse of 10s duration was applied, and then the potentiostat switched off. The slow scan axis was then re-enabled. This procedure was then repeated, allowing sequential images of the same area to be obtained. Given that during the experiment, the tip is only around 3 μm from the electrode surface, there is a possible concern about disturbance of nucleation and growth due to tip effects: it is informally acknowledged in the field of electrochemical SPM that the probe tip may "shield" the surface from unrestricted mass transport. In fact, no evidence for these effects were found in this system, as described later. A possible concern about using a technique that involves repeatedly switching the cell on and off is the time taken for steady-state diffusion to be achieved after the potential is applied. In fact, under the conditions of the experiment, this time was calculated as of the order of 0.2 s, short enough for the system to be in a steady state for almost all the deposition.[20]

TABLE 2: Rates of Nucleus Appearance at Various Potentials as Calculated from Potentiostatic Transients vs Values Observed Using AFM

		AFM	
potential/V	electrochemical N_0A/s^{-1}cm^{-2}	N_0A/s^{-1}cm^{-2}	N_0/cm^{-2}
−0.63	1.2×10^3	(1.7×10^3)	(1×10^5)
−0.67	6.2×10^3	3.7×10^4	1.6×10^6
−0.70	4.1×10^4	5.1×10^4	1.3×10^6
−0.73	6.2×10^4	5.4×10^4	3.2×10^6
−0.76	7.2×10^4		

Note that the AFM values for −0.63 V are an estimate, calculated assuming an N_0 of 1 nucleus per 30 μm^2 area.

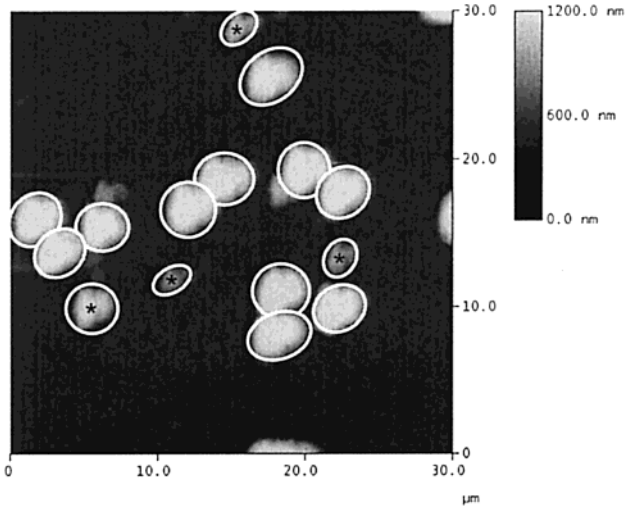

Figure 3. Final image in the set collected at −0.70 V (deposition for 160s). Ovals show the nuclei that were used for analysis purposes; those containing asterisks had a lower than predicted growth rate (see text).

The experiment was stopped when surface coverage reached an extent such that individual nuclei were impossible to resolve. The set of data obtained at −0.70 V are shown in Figure 2 as an illustration of the quality of the images obtained.

Nucleus Growth Rate. To analyze the resulting images, Digital Instruments Nanoscope software was used. This allowed detection of each particle above a threshold height, and calculated the base area and mean height of each particle. In every case, the threshold height was set consistently to a height allowing detection of the nuclei, but also reasonable noise removal (in all cases between 50 and 100 nm). To trace the growth of individual nuclei, the last image in each set was examined, and all the clear nuclei identified (as shown in Figure 3 for a potential of −0.70 V). These nuclei were then traced backward in time, and their area and height determined on each image, until the nucleus disappeared.

Multiplication of the nucleus base area by its mean height then allowed the nucleus volume, without recourse to assumption about the nucleus shape, to be plotted as a function of time, the results of which are shown in Figure 4. Note that at −0.63 V only one nucleus was observed. As a comparison, the theoretical diffusion controlled growth rate for a single nucleus, assumed to be hemispherical, is plotted in each case. This is calculated from the established equations for hemispherical diffusion[21]

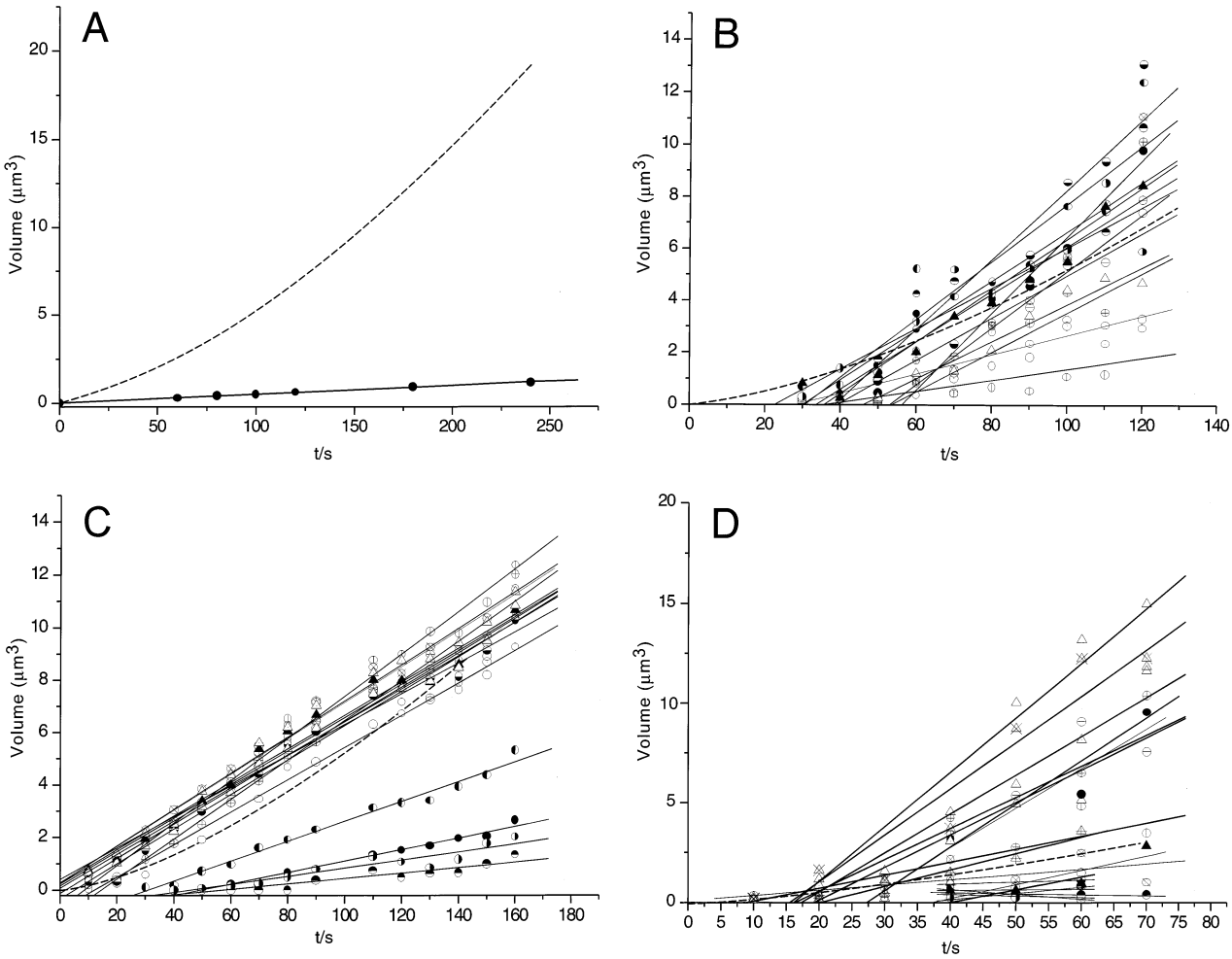

Figure 4. Nucleus volumes as a function of time at potentials of (A) −0.63 V, (B) −0.67 V, (C) −0.70 V, (D) −0.73 V. Thin lines show the lines of best fit for individual nuclei; Thick, dashed lines show the theoretical hemispherical diffusion controlled volume of a single nucleus calculated from eq 6.

$$\left(\frac{\partial V}{\partial t}\right) = \frac{2\pi r D c M}{\rho} \tag{6}$$

which integrates to give

$$V = \frac{4}{3}.2^{1/2}.\pi\left(\frac{M}{\rho}Dct\right)^{3/2} \tag{7}$$

where V is the volume of the nucleus.

Inspection of Figure 4 reveals many of the growth rates, at early times, are close to those expected for isolated nuclei (see theoretical curves shown in Figure 4 with the bold dashed line). There are notable exceptions: at −0.63 V, the growth rate of the single nucleus is much lower than the diffusion controlled rate; this is consistent with the system being under charge control at this potential. At higher overpotentials, there are some nuclei having a growth rate higher than the theoretical value, and some somewhat lower. The reason for this appears to be that some clustering of nuclei is occurring, making it difficult to separate nuclei clearly for analysis purposes. This is most often seen at −0.73 V, where the high nucleation rate causes the most nuclear overlap.

In most cases, the nuclei having a low growth rate are late appearing and close to another large, well-established nucleus, the effect of which is to reduce the local concentration of available Pb^{2+}. We may therefore conclude that at potentials above −0.63 V, the system is clearly under diffusion control and for individual, well spaced nuclei, the growth rate is very close to the expected value—*this result therefore represents a direct confirmation of the validity of eq* 6 *at a μm scale.* Equally when a large number of nuclei are present their interaction—via overlapping diffusion layers—serves to reduce the current as predicted approximately by the Scharifker and Mostany model.

Nucleation Rate and Saturation Nuclear Density. The number of nuclei on each image was also estimated as accurately as possible, given the problems of small nuclei being difficult to distinguish from noise, and nuclear overlap at long times. In most cases, the number observed was higher than the number used in the previous section, as some nuclei could be distinguished but were not well-defined enough for the volume to be determined. The resulting data, expressed as nuclei cm^{-2} are plotted in Figure 5. As only one nucleus was observed at −0.63 V, this has not been included. Note that in all cases, the experiments were continued long enough for the number of nuclei to appear to saturate. The results are consistent with the Sharifker and Mostany model, which predicts a linear increase in the number of nuclei until saturation, as is observed.

A linear best fit of the nucleus number density allows the approximate rate of nucleus appearance to be calculated. In fact, this is the same parameter as the N_0A derived from the current transient, and these are compared in Table 2.

At −0.67 V, the system is on the threshold of diffusion control, and is therefore particularly sensitive to ohmic drops in the cell, which may be estimated as up to 20 mV, a result of

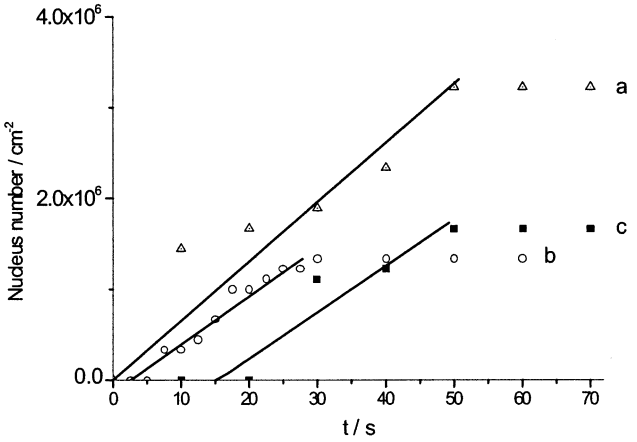

Figure 5. Nucleus number densities as a function of time at (a) −0.73 V, (b) −0.70 V, and (c) −0.67 V. Lines show best fits for the times before saturation.

the relatively large separation between the working and reference electrodes. Thus, we find a discrepancy in the values of N_0A at −0.67 V, whereas clearly in all of the other cases the values are in very good agreement.

Conclusions

The nucleation and growth rates of individual Pb nuclei on a BDD electrode were studied directly at various potentials above and below the onset of diffusion control, using in-situ AFM. This method removes the need for any chronoamperometric transient analysis, and therefore removes the need for any (arguable) assumptions about the growth rate of diffusion zones, nucleation rate laws, etc. Comparison between these new results and results derived from traditional transient analysis have therefore allowed the validity of transient analysis (in this case the SM model) to be tested, and excellent agreement was observed at potentials above the diffusion control threshold.

It was also demonstrated that the growth rate of individual nuclei (at potentials above −0.63 V) was well modeled by the expression for hemispherical diffusion limited growth. This confirms that the Scharifker and Mostany model can be correctly applied, as it requires diffusion control.

Finally, a re-expression of the Scharifker and Mostany equation for the current is suggested, which allows a less equivocal analysis of the rising transient part of the current response to be performed.

Overall, in-situ TappingMode AFM has been employed to directly examine the properties of individual growing nuclei on an electrode surface. It represents a new approach, as it requires no a priori assumptions to be made, unlike all previous analyses, which depended on interpretation of potentiostatic transients. The technique has clearly demonstrated its merits by independently verifying for the first time certain assumptions made by the SM equation, namely a diffusion controlled growth rate, and a constant nucleation rate.

References and Notes

(1) Gewirth, A. A.; Niece, B. K. *Chem. Rev.* **1997**, *97*, 1129.
(2) Magnussen, O. M.; Möller, F.; Vogt, M. R.; Behm, R. J. Nucleaton and Growth at Metal Electrode Surfaces. In *Electrochemical Nanotechnology*; Lorenz, W. J., Plieth, W., Eds.; Wiley-VCH: Weinheim, 1998.
(3) Iwata, F.; Saruta, K.; Sasaki, A. *Appl. Phys. A* **1998**, *66*, S463.
(4) Vidu, R.; Hara, S. *Scripta Materialia* **1999**, *41*, 617.
(5) Ikemiya, N. *Tetsu to Hagane* **1995**, *81*, N244.
(6) Ikemiya, N.; Yamada, K.; Hara, S. *Surf. Sci.* **1996**, *348*, 253.
(7) Koinuma, M.; Uosaki, K. *Electrochim. Acta* **1995**, *40*, 1345.
(8) Correia, A. N.; Machado, S. A. S.; Avaca, L. A. *J. Electroanal. Chem.* **2000**, *488*, 110.
(9) Scharifker, B.; Mostany, J. *J. Electroanal. Chem.* **1984**, *177*, 13.
(10) Sluyters-Rehbach, M.; Wijenberg, J. H. O. J.; Bosco, E.; Sluyters, J. H. *J. Electroanal. Chem. Interfacial Electrochem.* **1987**, *236*, 1.
(11) Mirkin, M. V.; Nilov, A. P. *J. Electroanal. Chem. Interfacial Electrochem.* **1990**, *283*, 35.
(12) D'Ajello, P. C. T.; Fiori, M. A.; Pasa, A. A.; Kipervaser, Z. G. *J. Electrochem. Soc.* **2000**, *147*, 4562.
(13) Ziegler, J. C.; Wielgosz, R. I.; Kolb, D. M. *Electrochim. Acta* **1999**, *45*, 827.
(14) Fletcher, S.; Halliday, C. S.; Gates, D.; Westcott, M.; Lwin, T.; Nelson, G. *J. Electroanal. Chem.* **1983**, *159*, 267.
(15) Heerman, L.; Tarallo, A. *J. Electroanal. Chem.* **1999**, *470*, 70.
(16) Scharifker, B. R.; Mostany, J.; Palomar-Pardave, M.; Gonzalez, I. *J. Electrochem. Soc.* **1999**, *146*, 1005.
(17) Cao, Y.; Searson, P. C.; West, A. C. *J. Electrochem. Soc.* **2001**, *148*, C376.
(18) Rigano, P. M.; Mayer, C.; Chierchie, T. *J. Electroanal. Chem.* **1988**, *248*, 219.
(19) Serruya, A.; Mostany, J.; Scharifker, B. R. *J. Chem. Soc., Faraday Trans.* **1993**, *89*, 255.
(20) Alden, J. A.; Hutchinson, F.; Compton, R. G. *J. Phys. Chem. B* **1997**, *101*, 949.
(21) Hills, G. J.; Schiffrin, D. J.; Thompson, J. *Electrochim. Acta* **1974**, *19*, 657.